Effect of Molecular Shape on Rheological Properties in Molecular Dynamics Simulation of Star, H, Comb, and Linear Polymer Melts

A. Jabbarzadeh,* J. D. Atkinson, and R. I. Tanner

School of Aerospace, Mechanical and Mechatronic Engineering, The University of Sydney, Sydney NSW 2006, Australia

ABSTRACT: A molecular dynamics simulation study has been conducted in order to shed light on the effect of molecular shape and structure on the rheological properties of linear and branched polymer melts. Couette shear flow has been simulated using Lees−Edwards sliding bricks periodic boundary conditions. Bulk properties of linear, star, H-shaped, and comb-shaped molecules have been calculated for many isomers of $C_{100}H_{202}$ polyethylene melt in order to do a controlled study on the effects of molecular architecture. Generally, branched polymers such as star, H, and comb-shaped molecules in non-Newtonian regime exhibit larger shear viscosities at high shear rates than their linear counterparts with the same molecular weight. However, the normal stress differences observed are higher for linear polymers. It is shown that while the shape of a molecule affects its rheological response, two important parameters, the effective length of the molecule and its degree of branching, ultimately dictate its response.

1. Introduction

The shape of molecules in liquids in general and polymer melts in particular dictates their dynamical behavior and rheological properties. Understanding these structural effects is crucial in synthesizing new polymers with desired properties. It is still very difficult to determine the structure of these polymers by experiments. Experimental techniques such as NMR are useful in determining the number of branches. However, in measuring the length of branches, NMR cannot differentiate branches that have more than 6−10 atoms.[1] Rheological responses of polymer melts have been used to determine molecular weight distributions (MWD).[2] Using highly active catalysts, we can control short- and long-chain branching.[3] This produces polymers with different rheological properties.[4] In the past the effect of molecular weight has been ignored in comparing branched polymers with different degrees of branching. Recent advances in synthesizing polymers have made it possible to produce polymers with almost the same molecular weight with different degrees of branching. Using these techniques in experiments with low-density polyethylene (LDPE) made by Wood-Adams,[5] an increased low-shear-rate viscosity was observed as the degree of branching was increased, while shear thinning began at lower shear rates. Commercial LDPE is usually polydisperse, and the molecular structure is irregular. For this reason developing a molecular theory to give quantitative results is beyond reach at present.[6] However, a great deal of theoretical work is being done on idealized branched polymers such as star and H-shaped molecules to generate molecular constitutive equations.[7,8] A molecular simulation such as the Monte Carlo method or molecular dynamics (MD) is an alternative approach. The advantage of these methods is that highly detailed architectures can be simulated with controlled molecular weight and shape of the molecules. However, the idealized molecules examined by these methods are usually much shorter than the real polymers. Usually, a limited number of molecules are examined in the simulation because of the large number of calculations required. Also, for

larger molecules the relaxation time is much longer and beyond the available simulation time. So the molecular weight of the simulated molecules is usually below the entanglement molecular weight. Although the molecules in these simulations are short, they can still capture much of the behavior of real polymer melts. These model molecules often reproduce nonlinear behavior and normal stress differences that are observed for polymer melts. MD simulations have shown that liquids that often appear Newtonian in experiments at low shear rates show non-Newtonian behavior if they are sheared at large enough shear rates, such as occur in MD simulations. Shear thinning is now thought to be a universal phenomenon at high enough shear rates. For molecules with long relaxation times shear thinning occurs at low shear rates, but for Newtonian fluids with very low relaxation times it happens at much larger shear rates. MD simulation can examine the properties of the fluid at very much higher shear rates than those possible to achieve in the laboratory. There are situations such as hard-disk lubrication and flow in nanochannels where the fluid experiences extremely high shear rates. So these simulations can also be used to capture the effect of molecular shape on the rheological behavior in such applications. And understanding of such structural effects no doubt can add to our knowledge and gives help in devising theoretical models for longer polymers.

Daivis and Evans[9] observed higher viscosity for branched alkanes in their shear simulation of linear and star-shaped C_{13} alkanes. Kioupis and Maginn[10,11] also investigated through MD the effect of molecular architecture on high-pressure rheology of lubricant molecules of C_{18} alkane. They investigated three types of molecules: one with the shape of a 3-arm star, one highly branched, and one a linear molecule. They observed differences in the viscosity index and viscosity dependence on the pressure and temperature for different structures. Khare et al.[12] studied the rheological response of three linear alkanes (C_{16}−C_{22}) and a branched (C_{22}) alkane. The only branched molecule that was simulated in this work showed higher viscosity than its

Table 1. Parameters for the Intramolecular and Intermolecular Interaction Potentials

(A) LJ potential		
CH$_3$, end group on the backbone	$\epsilon/k_B = 114$ K	$\sigma = 0.393$ nm
CH$_3$, side group	$\epsilon/k_B = 78$ K	$\sigma = 0.393$ nm
CH$_2$, all methylene groups	$\epsilon/k_B = 47$ K	$\sigma = 0.393$ nm
CH groups	$\epsilon/k_B = 32$ K	$\sigma = 0.385$ nm
(B) bending angle potential		
at CH$_2$ sites	$k_\theta = 520$ kJ/mol, $\theta_0 = 114°$	
at CH sites	$k_\theta = 520$ kJ/mol, $\theta_0 = 112°$	
(C) stretching potential	$k = 51\ 600\epsilon\sigma^{-2}$, $r_0 = 0.154$ nm	
(D) torsional potential		
X–CH$_2$–CH$_2$–Y (kJ/mol)	$C_0 = 9.2789$, $C_1 = 12.1557$, $C_2 = 13.1201$,	
	$C_3 = -3.0597$, $C_4 = 26.2403$, $C_5 = -31.4950$	
X–CH–CH$_2$–Y and X–CH–CH–Y (kJ/mol)	$C_0 = 3.4070$, $C_1 = 7.5003$, $C_2 = 1.6281$, $C_3 = -15.3732$	

linear isomer. In our earlier simulations on confined isomers of C$_{30}$ alkenes,[13] we investigated the effect of degree of branching on short lubricant molecules. Although the molecules were much shorter, the simulation results were very similar to experiments with LDPE[5] and hyperbranched polymers.[14] Our results showed an increase in the high-shear-rate viscosity of the confined film for branched molecules. We showed that viscosity increased with degree of branching. It is known that confined films behave differently compared to the same fluid in bulk. A systematic study on the effect of branching and shape is needed for bulk fluids. In the simulations that we present here we study the bulk properties of much longer molecules of C$_{100}$ isomers through MD simulation. The molecular weight of C$_{100}$ melt is 1425, which is 1–2 orders of magnitude smaller than that of commercial polyethylene. The number of possible isomers for C$_{100}$ is extremely large. However, from our earlier simulations we speculate that the shape of the molecule, number of branches, the length of the backbone, and also the length of the branches are important factors in designing the internal structure of molecules. We will study the shape effect by simulating star, H, and comb-shaped molecules. There are some experimental and theoretical works on these molecules that will be helpful in interpreting our results.

2. Simulation Details

We have conducted molecular dynamics simulations to simulate steady Couette shear flow using SLLOD[15,16] equations of motion and Lees–Edwards sliding brick boundary condition[17] for an NVT ensemble. The isothermal condition is achieved by using a Gaussian thermostat[16] directly applied to the equations of motion given by eq 1.

$$\dot{\mathbf{r}}_i = \frac{\mathbf{p}_i}{m} + \mathbf{e}_x \dot{\gamma} \mathbf{r}_{zi}$$

$$\dot{\mathbf{p}}_i = \mathbf{F}_i - \mathbf{e}_x p_{zi} \dot{\gamma} - \zeta \mathbf{p}_i \tag{1}$$

Here $\mathbf{e}_x$ is the unit vector in x direction (flow direction); $\mathbf{r}$, $\mathbf{p}$, m, $\dot{\gamma}$, and $\mathbf{F}$ are position vector, peculiar momenta, mass of each atom, shear rate, and the total force applied by the other atoms in the system. Coefficient ζ is the Gaussian thermostat given by eq 2:

$$\zeta = \frac{\sum_{i=1}^{N}(\mathbf{F}_i \cdot \mathbf{p}_i - \dot{\gamma} p_{xi} p_{zi})}{\sum_{i=1}^{N} \mathbf{p}_i^2} \tag{2}$$

An atomic thermostat is used in these simulations as it has been shown[18] for shear rates below $\dot{\gamma} \leq 2.5$ in reduced units ($\sim 1.1 \times 10^{12}$ s^{-1}) the choice of thermostat has no significant effect on the results of the calculation of rheological properties.

2.1. Model Liquid. A united atom model is used to model the alkane molecules. In this model, groups of CH, CH$_2$, and CH$_3$ are treated as single interaction sites. That is, carbon–hydrogen interactions are ignored by adjusting the mass and other parameters to compensate for them. We will refer to these groups as "atoms" for simplicity. Intramolecular architecture including bond stretching, angle bending, and torsional potentials are included in the model. These potentials are given respectively by the following equations.

$$\phi(r) = \frac{1}{2}k(r - r_0)^2 \tag{3}$$

$$\phi(\theta) = \frac{1}{2}k_\theta(\cos\theta - \cos\theta_0)^2 \tag{4}$$

$$\phi(\varphi) = \sum_{i}^{5} C_i(\cos\varphi)^i \tag{5}$$

The parameters for the intramolecular and also intermolecular potentials are given in Table 1. The equilibrium bond angle at a branch site of CH is slightly smaller than that for other groups. Also, for the torsional potential for X–CH$_2$–CH$_2$–Y (X and Y can be any group of atoms) interactions, the original Ryckaert–Bellemans[19] model is used since it has been shown[20] that the result does not change if the potential is replaced by values used in Siepmann et al.'s model.[21,22] For interactions that involve a branch site of tertiary carbon different parameters are used as prescribed in ref 21. The shifted Lennard-Jones (LJ) potential is given by eq 6

$$\phi_{LJ}(r) = 4\epsilon_{ij}\left[\left(\frac{\sigma_{ij}}{r}\right)^{12} - \left(\frac{\sigma_{ij}}{r}\right)^{6}\right] - \phi_{shift}$$

$$\phi_{shift} = 4\epsilon\left[\left(\frac{\sigma}{r_c}\right)^{12} - \left(\frac{\sigma}{r_c}\right)^{6}\right] \tag{6}$$

It governs the interactions of the atoms belonging to different molecules and also those of the atoms on the same molecule that are not interacting via intramolecular potentials given by eqs 3–5. Here ϵ and σ denote LJ energy and length parameters and r_c is the cutoff distance for potential calculations. A value of $r_c = 0.44$ nm is used in the simulations.

The parameters we have used have proven to produce results in good agreement with experiments for liquid–

vapor coexistence curves for linear and branched alkanes.[21,22] In this model, the Lennard-Jones energy parameter for methyl groups at the end of backbones is different from that for methyl groups at the end of branches. Also, different LJ parameters are used for a tertiary carbon CH group at the branch sites from those of a CH_2 group. These parameters for LJ interaction potentials are also given in Table 1. For the interaction of unlike groups Lorentz−Berthelot's combining rules are used so $\epsilon_{ij} = (\epsilon_i \epsilon_j)^{1/2}$ and $\sigma_{ij} = (\sigma_i + \sigma_j)/2$.

To eliminate the effect of molecular weight, we will study isomers of C_{100} with different shapes and degrees of branching. 3D snapshots and molecular structure of these molecules are shown in Table 2. To avoid their somewhat lengthy chemical names, we will refer these molecules with some generic names as indicated in Table 2. In this table the degree of branching (DB_1) is defined as the number of branches (i.e., number of branching points) per 100 carbon atoms of the molecule. The structure of the molecules and the positions of the branching points are also shown in these tables.

These simulations have been conducted in isothermal conditions where the fluid temperature is kept at 585 K, well above the melting point of a typical polymer melt such as HDPE. For all the simulations here the average density of the melt is 906 kg/m³. The simulation box dimensions for all the simulations were 6.904 × 5.178 × 5.178 nm in X, Y, and Z directions, respectively. This is sufficiently large, since a test run with a system 3 times bigger produced similar results. To generate the initial configuration, molecules were started on a simple lattice structure in a random conformation. The system then was melted and allowed time to equilibrate before applying the shear. The shear was applied in the XZ plane. Equations of motion were integrated by a leapfrog version of the Verlet algorithm. The time step used in the simulation was 4.709 fs for shear rates higher than $10^{8.5}$ s⁻¹ and 5.886 fs for shear rates lower than this value. The calculated relaxation time at zero shear rate for linear C_{100} simulated using similar parameters[23] is 3.3 ns, and we expect to have relaxation times of the same order here. The relaxation time for branched molecules is smaller than that of the linear molecule due to their smaller radius of gyration.[10] So our simulation duration (5−12 ns) is ∼1.5−4 times the maximum expected relaxation time. An equilibrium run of 300 000 time steps was performed followed by another 700 000 time steps to collect the results at higher shear rates. At lower shear rates we ran the simulations for 2 000 000 time steps. We performed the simulations by a domain decomposition parallel algorithm[25,26] on a cluster of Pentium IV workstations by using PVM (parallel virtual machine) message passing software that provided good speed-up and efficiency.

3. Calculated Properties

3.1. Stress Tensor. Stress tensor components can be calculated from the virial theorem by the Irving−Kirkwood[27] method. We have used an atomistic implementation of this method to calculate the stress tensor. According to this method, the contribution of each atom or particle to the stress tensor is in two parts, a kinetic part and a configuration part. This can be written as

$$\sigma_{xy} = -\frac{1}{V}\left\langle \sum_i^N m_i u_{ix} u_{iy} + \sum_i^N \sum_{j>i}^N r_{ijx} F_{ijy} \right\rangle \quad (7)$$

The first sum on the right-hand side of eq 7 is the kinetic contribution where m_i is the particle mass and x and y are coordination system axes which for a Cartesian system can be simply substituted by X, Y, or Z, and u_{ix} and u_{iy} are the peculiar velocity components of particle i in x and y directions. The second sum represents the configuration or potential contribution where r_{ijx} is the x component of the distance vector between particles i and j and F_{ijy} is the y component of the force exerted on particle i by particle j. N is the total number of atoms.

3.2. Shear Viscosity and Material Fuctions. The shear viscosity is calculated from the following definition from the shear stress (σ_{xz}) and shear rate

$$\eta = \frac{\sigma_{xz}}{\dot{\gamma}} \quad (8)$$

The first and second normal stress differences are calculated from the normal stresses using the following equations:

$$N_1 = \sigma_{xx} - \sigma_{zz}$$
$$N_2 = \sigma_{zz} - \sigma_{yy} \quad (9)$$

Total pressure is calculated from the normal stresses by eq 10.

$$P = -\frac{1}{3}(\sigma_{xx} + \sigma_{yy} + \sigma_{zz}) \quad (10)$$

4. Rheological Properties

We have conducted simulations for four types of molecules, namely linear, star, comb, and H-shaped molecules. For star, comb, and H-shaped molecules we varied the structural parameters such as the number of arms and branches and also the length of the branches to get an insight into the effect of each of those parameters. These molecules are shown in Table 2a,b together with their chemical structure, generic names, and degrees of branching.

4.1. Effect of Shape. Four isomers of $C_{100}H_{202}$ with linear, star, H, and comb shapes are simulated. These molecules are Chain100, Star100B4, HL52B12, and CombL52B4. The nominal backbone is used to map the structure of the molecules as given in Table 2a,b. The nominal backbone length of the H-shaped molecule defined as the length of the backbone between two branch points is 52. The length of each branch is 12 atoms for HL52B12. The comb-shaped molecule has a nominal backbone length of 52, and the length of each branch is 12 atoms. For Star100B4 there are two branching points next to each other along a nominal backbone of 50 atoms. So to a reasonable approximation it represents a star molecule with four arms of 25 atoms each. As a simple measure of the molecular size when stretched out by a strong flow, we introduce the effective length l_e, defined as the maximum distance (in terms of number of carbon atoms) between any two ends. Thus, the linear monomer Chain100 has $l_e = 100$, the star molecule Star100B4 has $l_e = 52$, the H-shaped molecule HL52B12 has $l_e = 76$, and the comb molecule Comb52B4 has $l_e = 64$. This is shown for an H-shaped molecule in Figure 2.

4.1.1. Shear Viscosity. The shear viscosity for shear rates from $10^{7.5}$ to 10^{12} s⁻¹ using eq 8 is given in Figure 1 on a logarithmic scale. We can see that at higher shear rates the viscosity is larger for branched molecules

Table 2. 3D Snapshot, Chemical Structure, Generic Name, and Degree of Branching for the Molecules Simulated Here[a]
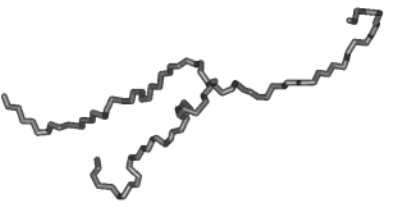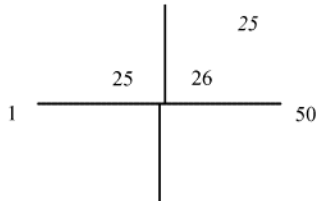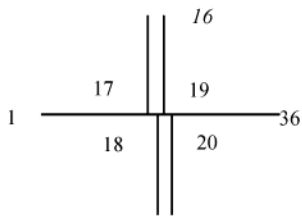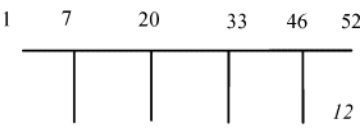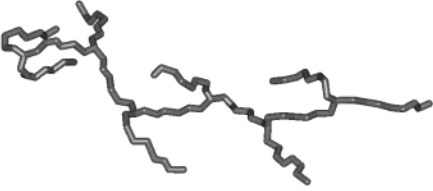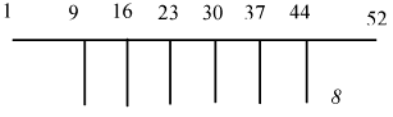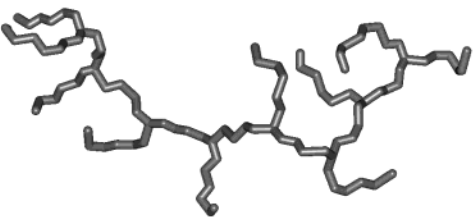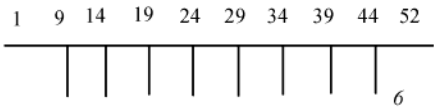
Molecular Structure and a 3D snapshot	Chemical Structure	Generic Name	DB_1
	$C_{100}H_{202}$	Chain100	0
	33 / 1 34 67	Star100B3	1
	25 / 25 26 / 1 50	Star100B4	2
	16 / 17 19 / 1 36 / 18 20	Star100B6	4
	1 7 20 33 46 52 / 12	CombL52B4	4
	1 9 16 23 30 37 44 52 / 8	CombL52B6	6
	1 9 14 19 24 29 34 39 44 52 / 6	CombL52B8	8

Table 2 (Continued)

		HL28B18	4
		HL52B12	4
		HL76B6	4

[a] There is a linear molecule together with three star-type, three comb-shaped, and three H-shaped molecules. In the chemical structure shown for the molecules the numbers show the position of the branches along the nominal backbone and also the end points of the nominal backbone. Italic numbers next to the branches indicate their length (excluding the branch point).
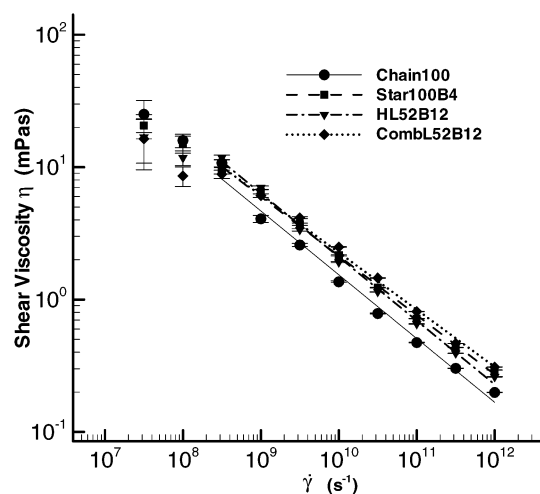

Figure 1. Shear viscosity vs shear rate for four different isomers of $C_{100}H_{202}$ with different shapes. Star molecule has 4 arms of 25 atoms each; HL52B12 and CombL52B12 also have 4 branches of 12 atoms each. Chain100 is a linear molecule.
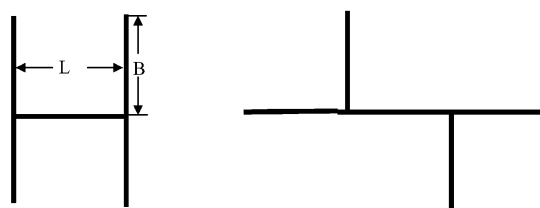

Figure 2. An H-shaped molecule with a nominal backbone of L and four branches of length B can be reshaped to a molecule with effective length of $L + 2B$ with two branches of B.

compared with the linear molecule. For branched molecules the viscosity is up to twice as large as that of the linear molecule. This is similar to that observed in simulation of a branched alkane (2,5-dipropylhexadecane).[12] Daivis and co-workers[9] simulated $C_{13}H_{28}$ alkane and observed higher viscosity for 3-arm star, 5-butyl-nonane compared to tridecane, its linear isomer. Shear viscosity enhancement was observed for confined C_{30} alkane branched molecules[13] and also for shorter branched C_{18} alkanes.[11] In our simulations all the molecules have the same molecular weight so the results only differ because of the shape effect. It is seen that the shear viscosities of the star and H-shaped molecules are similar, though slightly higher for the former. The

Table 3. Shear Viscosity Is Tabulated from High to Low at Shear Rates of $10^{10.5}$ s^{-1} and $10^{9.5}$ s^{-1} for All Molecules[a]

molecule	η (mPa s) $\dot{\gamma} = 10^{10.5}$	η (mPa s) $\dot{\gamma} = 10^{9.5}$	N_1 (MPa) $\dot{\gamma} = 10^{9.5}$	R_g^2 (nm^2) $\dot{\gamma} = 10^{9.5}$	l_e	α	β	DB_1	DB_2	DB_3
combL52B8	1.889	5.300	19.573	1.233	52	0.44	0.63	8	15.4	29.6
combL52B6	1.704	5.006	17.268	1.395	52	0.42	0.62	6	11.5	22.2
star100B6	1.527	4.225	14.045	0.944	36	0.41	0.81	4	11.1	30.9
combL52B4	1.457	4.151	20.308	1.841	64	0.43	0.60	4	6.3	9.8
star100B4	1.228	3.709	16.793	1.573	52	0.45	0.72	2	3.9	7.4
HL28B18	1.181	3.559	17.872	2.140	64	0.46	0.66	2	3.1	4.9
HL52B12	1.144	3.460	22.853	3.077	76	0.48	0.61	2	2.6	3.5
HL76B6	1.073	3.363	35.002	4.666	88	0.47	0.57	2	2.3	2.6
star100B3	1.042	3.165	17.054	2.233	66	0.46	0.67	1	1.5	2.3
chain100	0.785	2.583	20.225	5.567	100	0.49	0.54	0	0	0

^{a} α and β are the exponent in power-law region for shear viscosity and first normal stress difference. The statistical error for the viscosity values is 0.07–0.09 for shear of $10^{9.5}$ s^{-1} and 0.01 or less for $10^{10.5}$ s^{-1}. The mean-squared radius of gyration R_g^2 is calculated at $\dot{\gamma} = 10^{9.5}$ s^{-1}. The degree of branching is given for each molecule based on three definitions. The effective backbone length l_e is the number of carbon atoms along the longest distance between any two free ends of the molecule.

shear viscosity of the comb-shaped molecule is larger again at the higher shear rates. However, at the lower shear rates ($10^{8.5}$ s^{-1} and below), the statistical uncertainty due to thermal motion is too large to evaluate the results accurately; our simulation time is not long enough to get good averages in this regime. At shear rates above $10^{8.5}$ s^{-1} the results seem more consistent. For all the molecules shear thinning is observed. For most of them, the onset of shear thinning appears to occur at considerably lower shear rates than we were able to examine here, that is, somewhat below $10^{8.5}$ s^{-1}. For the smaller confined molecules (C_{30}) that we studied before,[13] we were able to observe the onset of shear thinning at about $10^{9.2}$ s^{-1}, with a Newtonian regime at lower shear rates. For bead–spring molecular models with Hookean springs, the onset of shear thinning occurs at shear rate of order λ^{-1}, where λ is the longest relaxation time, and is proportional to the number of beads. Thus, we would expect the onset of shear thinning for C_{100} at about $10^{8.7}$ s^{-1} in our case. On the basis of the Rouse theory[32] and the calculated relaxation time, Moore et al.[23] predicted the onset of shear thinning at about $10^{8.5}$ s^{-1} for linear C_{100} molecules. However, this was not clear in the MD results that were provided in that work. We also find somewhat lower values than the Rouse model prediction in the present investigation, although conditions here are not completely comparable.

We have fitted the viscosity data to a power law in the region where the shear rate is higher than $10^{8.5}$ s^{-1}, where the statistical errors are small. For all the molecules the viscosity is proportional to a power of shear rate: $\eta \propto \dot{\gamma}^{-\alpha}$ where, however, the exponent α seems to be a function of the type of molecule. Table 3 gives these exponents. Also listed in Table 3 are three measures of the degree of branching: DB_1, the number of branch points per 100 atoms; DB_2, the number of branches per 100 atoms of the effective length ($DB_2 = DB_1 \times 100/l_e$); and DB_3, the number of branches divided by the square of this quantity ($DB_3 = DB_1 \times (100/l_e)^2$). DB_2 and DB_3 are thus greater for molecules with longer branches and thus a shorter "effective backbone". The effect of shape on shear viscosity is well characterized by DB_1, since the star and H-shaped molecules (both with $DB_1 = 2$) have very similar shear viscosity and the linear molecule ($DB_1 = 0$) has lower viscosity, while the comb molecule ($DB_1 = 4$) has higher shear viscosity at high shear rates. This increase of shear viscosity at high shear rates with the degree of branching, together with slightly weaker shear thinning effect (smaller α), agrees with experimental results with long-chain branching molecules (at much higher N) (see below). Since the

point of onset of shear thinning in each case was not accurately determined, we are unable to comment on how it correlates with degree of branching.

In experiments with low-density polyethylene (LDPE) made by Wood-Adams,[5] the low-shear-rate viscosity increased and shear thinning began at a higher shear rate as the degree of branching was increased. In that work a technique was employed to synthesize samples with almost the same molecular weight with different degrees of branching. Sendijarevic and McHugh[14] have performed experiments with high-molecular-weight hyperbranched polymers of polyesters and poly(ether–imide) with various degrees of branching. Interestingly, their findings are in agreement with our findings showing the shear-thinning effect becomes weaker as the degree of branching is increased. Despite the much lower shear rates (1–100 s^{-1}) used in the mentioned experiments[5,14] with long polymers, their results correspond well with ours. In fact, the relaxation time for the long, high molecular weight, and hyperbranched molecules that they have tested is many orders higher than the short molecules that we have examined here. So the high shear rates we have used here are offset to some extent by their long relaxation times.

4.1.2. Normal Stress Differences. The first normal stress difference N_1 is plotted in Figure 3 for the same four cases as before. N_1 is positive in all cases. As the shear rate increases, there is significant enhancement of N_1, which follows a power law with shear rate of form $N_1 \propto \dot{\gamma}^\beta$ as shown by straight lines in the graph. The exponent β, however, seems to be larger for branched molecules as can be seen from Table 3. At shear rates below $10^{8.5}$, N_1 seems to be larger for the linear molecule than for the branched molecules. At higher shear rates the H-shaped molecule has higher N_1. The reason is that as the shear rate increases, the H-shaped molecule stretches under the flow and reaches its effective backbone length of 76. It seems the effective length of the molecule plays an important role here. For star-shaped molecules the effective length does not change under flow and remains the same (52 atoms). For CombL52B4 the effective backbone length is 64 atoms. From closer inspection of the results we find that N_1 is slightly larger for CombL52B4 molecule in comparison to that of Star100B4. This should also explain the higher first normal stress difference observed for HL52B12 in comparison to Star100B4 and CombL52B12 molecules. Backbone length, though, cannot explain why the H-shaped molecule exhibits larger values for N_1, as the effective backbone length of H-shaped molecules are shorter than that of Chain100. It seems this result is
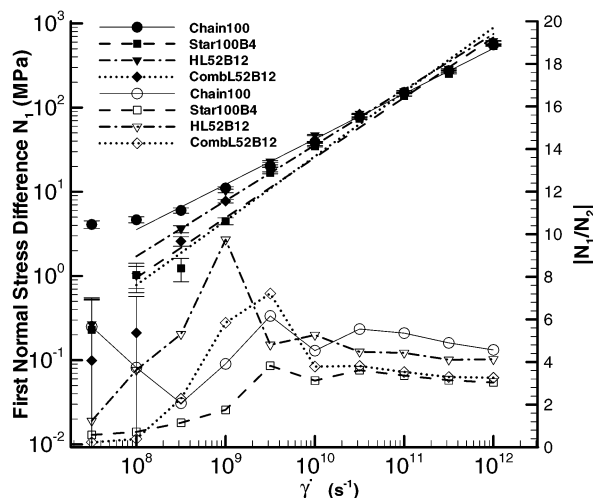
Figure 3. First normal stress difference and normal stress difference ratio against shear rate for four isomers of $C_{100}H_{202}$ molecules. The filled symbols are for N_1, and open symbols are for $|N_1/N_2|$. The error bars for $|N_1/N_2|$ are not shown here to enhance the clarity of the results. The errors are smaller than the symbols for $\dot{\gamma} > 10^{10}$ s^{-1}. For $\dot{\gamma} < 10^{10}$ the errors are larger ($\sim 0.6-7$).

somehow related to the shape of the molecule and lengths of the branches. We will study this further for other shape molecules in the coming sections.

We also calculated the second normal stress difference N_2, which was negative for all cases. The absolute value of the ratio $|N_1/N_2|$ is plotted against shear rate in Figure 3. At shear rates below 10^{10} s^{-1} the statistical errors are large since N_2 is the difference of two small quantities, and the peak in $|N_1/N_2|$ is probably attributable to this error. At higher shear rates there is a plateau region with much smaller errors, and the ratio here is $4-6$, which is consistent with that observed in experiments with polyethylene[29] where it is found that $|N_1/N_2| \sim 4$. At this region $|N_1/N_2|$ is the largest for the linear molecule followed by the H-shaped molecule, while the star and comb-shaped molecules have very similar values for this ratio, with that for the comb-shaped molecule being slightly higher. It seems that the effective length of the molecule, as characterized by l_e, is an important factor here. For the linear molecule $l_e = 100$, followed by the H-shaped molecule with $l_e = 76$, the comb-shaped molecule with $l_e = 64$, and finally the star with $l_e = 52$. This is the same order as that of $|N_1/N_2|$.

4.1.3. Pressure. Figure 4 shows the total pressure for the same linear, star, H, and comb-shaped molecules as before. The linear molecule initially exhibits a pressure drop as the shear rate is increased, with a minimum at a shear rate between $10^{10.5}$ and 10^{11} s^{-1}, and a rapid increase at higher rates. The drop in pressure for the linear molecules is as much as 45 MPa or about 5%. The branched molecules have about the same pressure at low shear rates, but it has only a small drop as shear rate increases, followed by the same rapid increase as the linear molecule, starting at somewhat lower shear rates.

Khare et al.[12] also observed this pressure drop for shorter linear alkanes of C_{28} and C_{16}, although it was absent for a branched C_{22} (DPHD). In their results the pressure drop seemed to be greater for C_{28}, suggesting that it is dependent on the molecular length, specially since the drop for our C_{100} molecules is even larger.
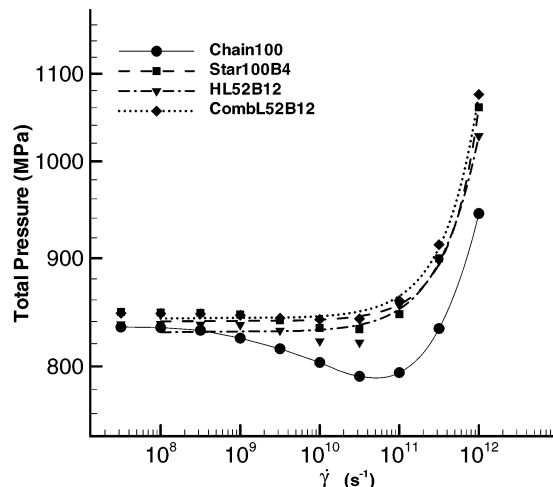

Figure 4. Total pressure against the shear rate for linear, star, H, and comb-shaped isomers of $C_{100}H_{202}$.

Daivis and Evans[9] did not observe any pressure drop in their simulation of a short C_{13} alkane. Moore et al.,[23] simulating C_{100} chains at lower density and temperatures, observed the same pressure drop as us at about the same shear rates. They attributed this pressure drop to a minimum in the LJ potential energy at about the same shear rate. In all, comparing our results with previous works, we conclude that the length of the molecule is an important parameter governing the pressure drop for linear molecules, while our results together with those of Khare et al. suggest that for molecules with branches this effect is much smaller, even for long molecules.

4.2. Effect of Number of Branches. To examine the effect of the number of branches on the rheology of each shape, we did simulations with star-shaped molecules with 3, 4, and 6 arms of approximately equal length and with comb-shaped molecules with 4 branches each of length 12, 6 branches of length 8, and 8 branches of length 6. Thus, each comb has about the same effective length. Note that the molecular model in our simulation allows a maximum of 3 carbons to attach to each "atom". (Four is theoretically possible, but unlikely for large molecules.) Thus, for stars with more than three arms there must be more than one branch point, though these points are placed next to each other so as to mimic an ideal multiarmed star as closely as possible. See Table 2 for full details of the structure of all these molecules, together with DB_1, the degree of branching. The latter varies from 1 for the 3-armed star to 8 for the 8-branch comb.

4.2.1. Effect of Number of Branches on Shear Viscosity. For the three star molecules, the results for shear viscosity against shear rate are presented in Figure 5. At higher shear rates where the statistical uncertainties are small enough to draw conclusions, it can be seen that the viscosity increases consistently as the number of arms and thus the degree of branching DB_1 is increased. This result is consistent with the results of experiments on star molecules of polyisoprene polymer,[28] although in that reference the molecular weight of the molecules varied, while the molecular weight of each arm remained the same. The exponent when a power law is fitted to the shear thinning curves is shown in Table 3. It can be seen that as the degree of branching increases the exponent decreases, indicating a weaker shear thinning.
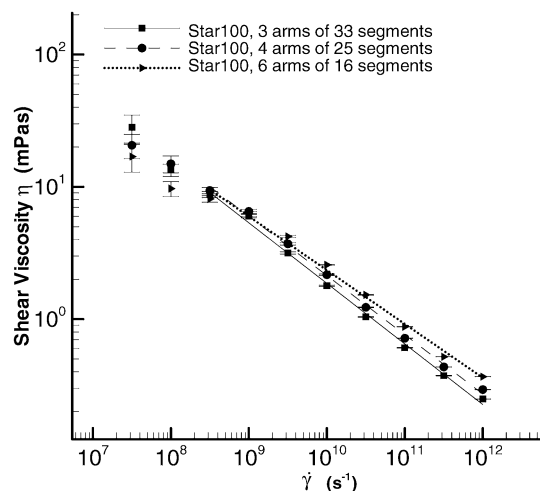
Figure 5. Shear viscosity against the shear rate for star type molecules with different numbers of arms. Stars with 3, 4, and 6 arms are plotted here.
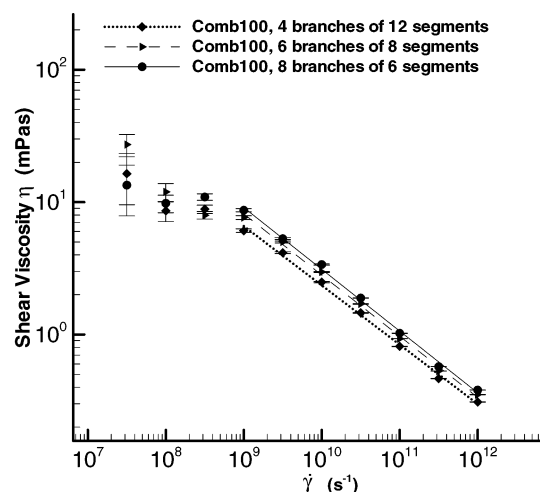

Figure 6. Shear viscosity is plotted against the shear rate for three comb-type molecules with different number of branches (see Table 2).

For the three comb-shaped molecules, the shear viscosity is plotted against shear rate in Figure 6. Again, the viscosity increases consistently with the number of branches. The transition from Newtonian behavior to shear thinning behavior appears to be occurring at higher shear rates for combs than for stars, while no significant variation in the power-law exponent α can be seen as number of branches varies (see Table 3).

Looking at all these results together suggests it is the degree of branching rather than effective length that determine shear viscosity, at least at the higher shear rates. The comb molecules all have l_e about the same (52−64), and the molecular weight is the same, so the increase in viscosity must be due to the variation in DB_1. For stars, the effective length decreases inversely proportional to the degree of branching. However, the viscosity still increases. At lower shear rates it appears that the tendency is reversed for stars—the viscosity for the star with 6 arms seems particularly low here. It is not clear whether this means that effective length has more effect than degree of branching at lower shear rates or whether the larger statistical inaccuracies at low shear rates are leading to errors.

4.2.2. Effect of Number of Branches on Normal Stress Differences. The results for first normal stress
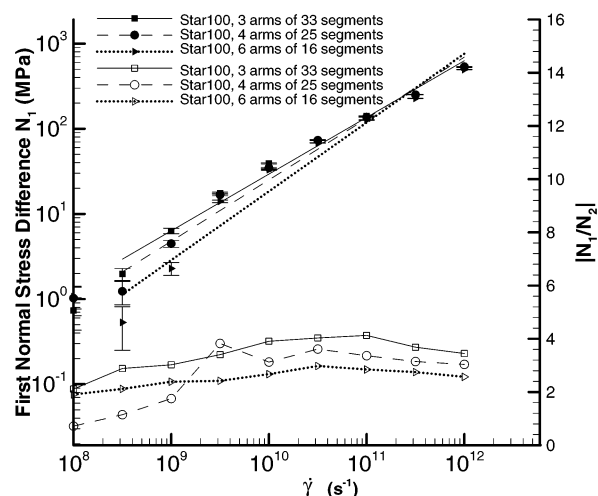

Figure 7. First normal stress difference and normal stress difference ratio against the shear rate for three different star type molecules with 3, 4, and 6 arms. All molecules have the same molecular weight. The filled symbols are for (N_1), and open symbols are for $|N_1/N_2|$. The error bars for $|N_1/N_2|$ are not shown here to enhance the clarity of the results. The errors are smaller than the symbols for $\dot\gamma > 10^{10}$ s^{-1}. For $\dot\gamma < 10^{10}$ the errors are larger ($\sim$0.6−1.3).
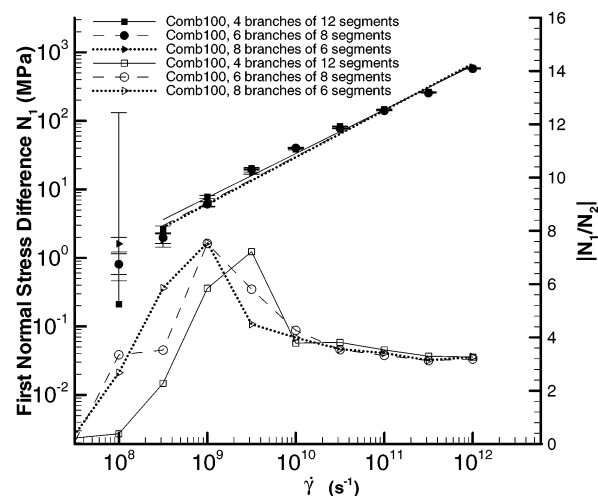

Figure 8. First normal stress difference and its ratio with second normal stress difference vs shear rate for three comb-shaped molecules. All the molecules have the same molecular weight. The filled symbols are for N_1, and open symbols are for $|N_1/N_2|$. The error bars for $|N_1/N_2|$ are not shown here to enhance the clarity of the results. For $\dot\gamma < 10^{10}$ the errors are large ($\sim$1−7). The errors are smaller than the symbols for $\dot\gamma > 10^{10}$ s^{-1}.

difference for the three star molecules with 3, 4, and 6 arms are plotted in Figure 7. At lower and intermediate shear rates the first normal stress difference drops as the number of arms increases. It appears likely that this is connected to the decrease in effective backbone length as the degree of branching increases. The results for comb-shaped molecules with similar l_e, as shown in Figure 8 are almost indistinguishable at intermediate and high shear rates. This confirms that the effective backbone length of the molecule (l_e), which governs how far the molecule can be stretched out, is the dominant factor in determining the normal stress difference and that the degree of branching is much less important.

The ratio of first and second normal stress difference, $|N_1/N_2|$, is given on the same figures. At lower shear rates nothing much can be said because of statistical
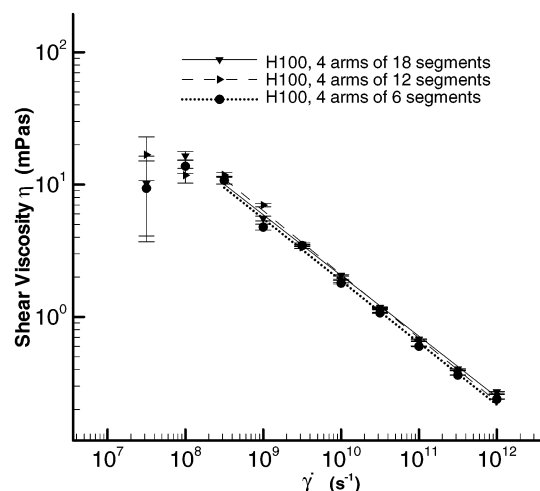
Figure 9. Shear viscosity for three H-shaped molecules with different branch lengths. The effective length increases as the branch length decreases.

Figure 10. First normal stress difference and its ratio with the second normal stress difference against the shear rate for three H-shaped molecules described in section 4.3. The filled symbols are for N_1, and open symbols are for $|N_1/N_2|$. Note the effective length of the molecule decreases as the length of the branches is increased. The error bars for $|N_1/N_2|$ are not shown here to enhance the clarity of the results. The errors are smaller than the symbols for $\dot{\gamma} > 10^{10}$ s^{-1}. For $\dot{\gamma} < 10^{10}$ the errors are larger ($\sim$2$-$7). The spike seen for $|N_1/N_2|$ seems to be due to large error in that area.

inaccuracies, but at higher shear rates of 10^{10} s^{-1} upward the ratio remains fairly constant at about 2.5$-$4 for both star and comb-shaped molecules. For the star molecules, the ratio is higher when there is less branching and therefore a greater effective length. For the comb-shaped molecules, with similar l_e but different degrees of branching the three curves are almost identical at the higher shear rates. Thus, it appears that l_e is again the dominant factor in determining the ratio of normal stress differences.

4.3. Effect of the Length of Branches. To measure the effect of branch length, we performed simulations using three different H-shaped molecules of $C_{100}H_{202}$. For these, the degree of branching remains the same (DB$_1$ = 2 in each case) and the branch length varies widely, taking values of 18, 12, and 6 in the three cases, while to maintain the total number of atoms at 100, the effective length varies inversely to this, taking values of 64, 76, and 88, respectively.

4.3.1. Effect of the Length of Branches on the Shear Viscosity. Shear viscosity is plotted against shear rate in Figure 9. At shear rates higher than $10^{8.5}$ s^{-1}, all three curves are very close. Examining the numerical values in Table 3, we see that the viscosity increases as the length of branches increases. But the effect is small, less than the effect of number of branches we found for star and comb-shaped molecules. Non-Newtonian shear thinning occurs, and as usual, it is not possible to detect the point of transition from the Newtonian regime due to the statistical inaccuracy of the results at the lower shear rates.

In section 4.1.1, we defined three measures of degree of branching: DB$_1$, which (for molecules of the same molecular weight) simply measures the number of branch points; and DB$_2$ and DB$_3$, which measures branch points per effective length and per effective length squared. While DB$_1$ is the same for all three H-shaped molecules, DB$_2$ increases as branch length increases (but more slowly) and thus correlates quite well with the shear viscosity. However, the viscosities of the molecules with length of 12 and 18 differ only slightly. Does this mean that beyond a certain branch length, relative to molecular size, branch length does not affect viscosity much? Compare with comb-shaped molecules (section 4.2.1), where both number of branches
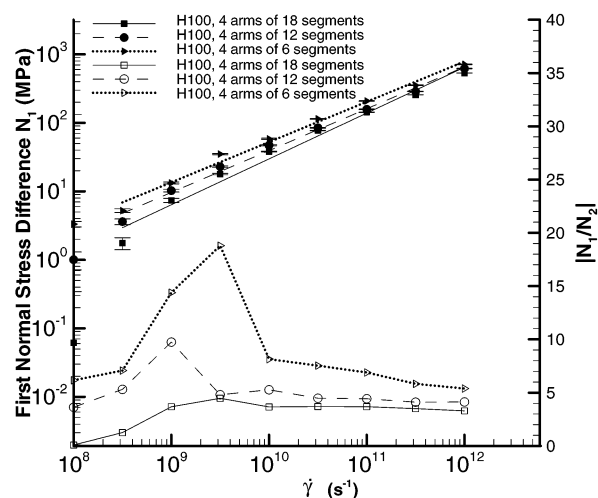
and branch length vary and where shear viscosities differ by a much larger amount. We speculate that the number of branches has a greater effect on viscosity than their length and that the effect of branch length becomes small once it becomes more than a few atoms.

4.3.2. Effect of the Length of Branches on First Normal Stress Difference. Figure 10 shows N_1 for the three H-shaped molecules described in section 4.3. We see that N_1 is larger for the molecules with the shortest branch length, namely 6, and that the normal stress difference decreases as the length of branch increases. Equivalently, normal stress difference increases as effective length increases. Since l_e determines the distance the molecule can be stretched out, it appears that, as in the case of star molecules, l_e is the dominant factor determining N_1. Although we cannot rule out that the length of each individual branch has a direct effect, especially when it is stretched out by the shear, we think the overall length is more important. The ratio of normal stress differences, $|N_1/N_2|$ is also plotted in Figure 10. We see that, above a shear rate of about $10^{9.5}$, the curves form a plateau at values of about 3$-$7. The molecules with shorter arms, corresponding to longer l_e, have higher values of $|N_1/N_2|$ in this region. This agrees qualitatively with conclusions made previously, that the ratio depends mainly on l_e rather than degree of branching. However, from Figures 3 and 10 it is seen that the ratio for the linear molecule, though large (about 5), is noticeably smaller than that for the H-shaped molecule with the shortest arms (6$-$7.5), despite the fact that its value of l_e is larger (100 as against 88). We are unable to account for this discrepancy. To clarify the effect of the molecular length on the normal stress differences, we simulated a shorter linear molecule of C_{50} and plotted the first normal stress difference and also normal stress difference ratio for this molecule and linear C_{100} in Figure 11. We can clearly see in this picture that both N_1 and $|N_1/N_2|$ are larger for the longer molecule.
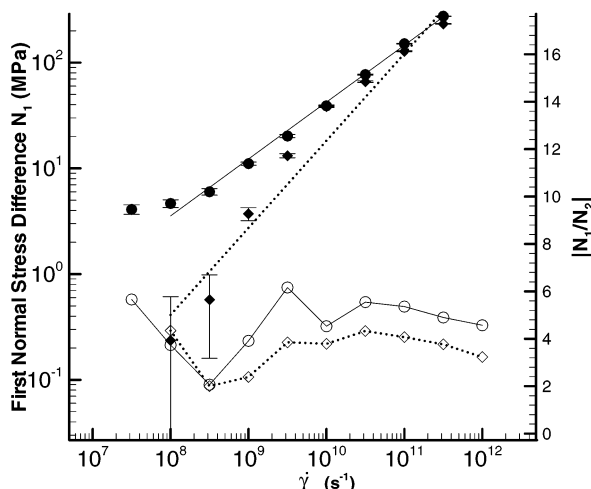
Figure 11. First normal stress difference (filled symbols) and normal stress difference ratio (open symbols) for two linear molecules of C_{50} (diamonds) and C_{100} (circles).
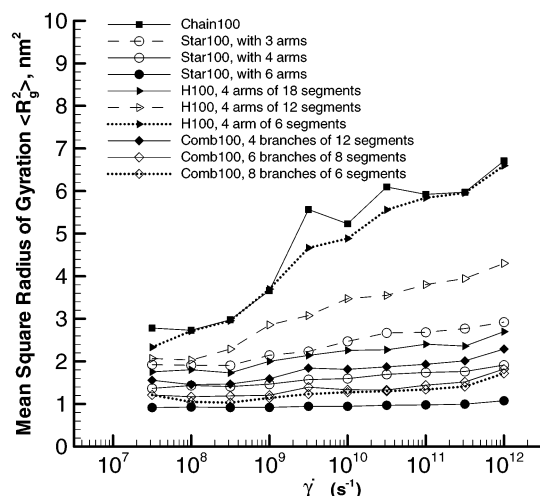

Figure 12. Mean-squared radius of gyration against the shear rate for all the molecules simulated. All the error bars are smaller than the symbols and are not shown here.

5. Structural Properties

We have calculated the radius of gyration for the molecules from the following expression:

$$\langle R_g^2 \rangle = \left\langle \frac{\sum_i m_i |\mathbf{r}_i - \mathbf{r}_{cm}|^2}{\sum_i m_i} \right\rangle \tag{11}$$

where m and $\mathbf{r}$ are the mass and position of each atom on the molecule and $\mathbf{r}_{cm}$ is the center of mass of the molecule. The results are depicted in Figure 12 for all the molecules simulated in this work. We can see that for the linear molecule the radius of gyration increases as the shear rate is increased. For H-shaped molecules the radius of gyration decreases as the lengths of the arms are increased. (This is expected since the nominal backbone is decreased.) For H-shaped molecules the effect of shear on the radius of gyration decreases as the nominal backbone length is decreased. For comb and star molecules the influence of shear rate on the radius of gyration is smaller. For a star with six arms R_g^2
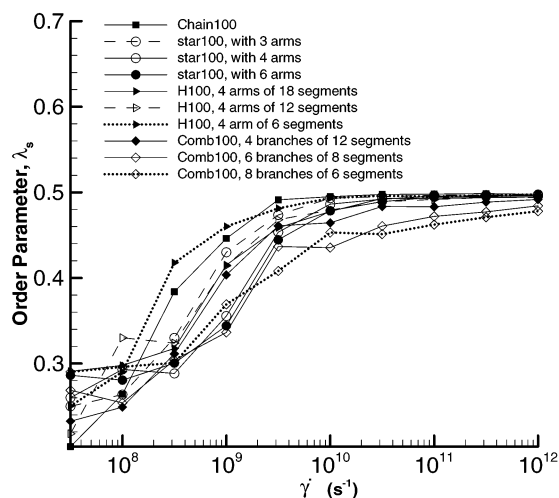

Figure 13. Order parameter for all the molecules against the shear rate. The error bars are smaller than the symbols and are not shown for clarity.

almost remains unchanged at even high shear rates. The Rouse theory[32] for unentangled short chains predicts that R_g^2 is proportional to the rotational relaxation times of the molecule and the relaxation time is proportional to the viscosity. So the viscosity should scale up with radius of gyration. We do not get the same picture as the Rouse model would have predicted, and it seems our results are more similar to the results of Kioupis and Maginn[10] for shorter C_{18} where the same discrepancy was observed.

We have also calculated the order tensor[9] **S** given as

$$\mathbf{S} = \frac{3}{2} \left\langle \frac{1}{N} \sum_{i=1}^N \left(\mathbf{u}_i \mathbf{u}_i - \frac{1}{3}\mathbf{I} \right) \right\rangle \tag{12}$$

where $\mathbf{u}_i$ is the unit vector along the longest axis of inertially equivalent ellipsoid for the molecule and $\mathbf{I}$ is the unit tensor. The longest axis is the eigenvector corresponding to the smallest eigenvalue of the inertia tensor of the molecules. The order tensor is a traceless tensor, and its largest eigenvalue is called the order parameter λ_s. The order parameter can have any value between 0 (disorder) and 1 (perfect orientation order). It is usually used as a measure of the shear-induced alignment of the molecules in shear flow. We have plotted the order parameter against the shear rate for all the molecules that we simulated here in Figure 13. It is known that the alignment of the molecules in the flow direction is responsible for the shear thinning observed. From Figure 13 we can see that at lower shear rates λ_s increases with the radius of gyration of the molecule where linear and H-shaped molecules have the lowest value for λ_s, followed by and star and comb-shaped molecules. At higher shear rates λ_s converges for all the molecules except for comb-shaped molecules, although the same dependence on the radius of gyration remains. Ordering of the molecules increases with shear rate for all the molecules and then reaches a plateau at higher shear rates. For linear and H-shaped molecules this plateau is reached at lower shear rates, which possibly explains the steeper rate of shear thinning behavior for these cases. The star and, to a greater degree, comb-shaped molecules reach the plateau at higher shear rates. This could be an indication that these molecules shear thin at larger shear rates al-
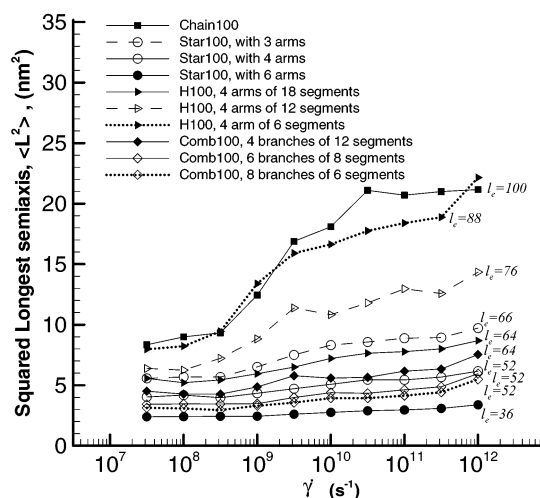
Figure 14. Time-averaged squared longest semiaxis of an inertially equivalent ellipsoid that represents the molecule. The effective length of the molecule in given by l_e next to each molecule.

though this plateau is reached at higher shear rates than those where shear thinning starts. In fact, for most of the molecules the onset of the Newtonian regime appears to occur at lower shear rates than we were able to detect clearly.

It is always possible to find an ellipsoid that represents the molecule. This ellipsoid has a uniform density with the same moment of inertia tensor as of the molecule.[9] We have plotted the mean-squared longest semiaxis $\langle L^2 \rangle$ of this ellipsoid against the shear rate in Figure 14. L^2 changes with the shear rate similar to radius of gyration. The longest semiaxis is a measure of effective length of the molecule. This can be seen from Figure 14 where the effective backbone length of the molecules is also shown. It can be seen the effective length increases so does the longest semiaxis. Also, the radius of gyration is correlated with the effective length in the same way. We have used the "effective length" in our discussions because it can be more easily determined from the shape of the molecule by simply counting the number of atoms along the longest possible backbone of the molecule.

6. Discussion and Conclusions

We performed molecular dynamics simulations of model polymer melts in shear to establish the effect of important structural parameters on the rheological properties. We simulated many isomers of $C_{100}H_{202}$ molecules in a bid to understand the effect of shape and degree of branching on the results. We obtained the bulk properties such as shear viscosity, first normal stress difference, and normal stress difference ratio for these model polymers. Simulations provided results only in the non-Newtonian regime due to the large size of the molecules. We found that the shape of the molecule has important effects on the final properties of the polymer melt. For linear molecules Rouse theory predicts that the viscosity scales up with the radius of gyration. It seems this is not true for the branched molecules in the non-Newtonian regime that we simulated here. In fact, the opposite is true here to some extent although it is not consistent in all cases—refer to Table 3 where shear viscosity and radius of gyration are listed for all the molecules. It seems that in the case of branched molecules other factors have more influence on the trend

in viscosity. We found that two important geometrical parameters are the degree of branching and the effective length of the molecule. The effective length of the molecule is proportionate to both the radius of gyration and the longest semiaxis of an inertially equivalent ellipsoid. However, it offers a more convenient measure of size of the molecule since it can be determined directly from the molecular architecture. In our simulations we found that in the non-Newtonian regime the branched molecules generally exhibit larger shear viscosity than that of their linear counterpart. Star molecules with different number of arms were examined, and we found that the shear viscosity increased with the number of arms. Also, we found that for the comb-shaped molecules as the number of branches increased so did the shear viscosity. This was a direct result of the increased degree of branching, as molecular weight and nominal backbone length were the same for all comb-shaped molecules and the effective length was almost the same. The increased shear viscosity observed here is consistent with the experimental measurements.[28,30] The question is whether can we define a single parameter that to a large degree qualitatively predicts the viscosity from structural parameters. We introduced three definitions for degree of branching DB_1, DB_2, and DB_3 based on the effective length of molecule and the number of branches. To test which one of these parameters most accurately predicts the viscosity, we have tabulated the viscosity we calculated at shear rates of $10^{9.5}$ s^{-1} and $10^{10.5}$ for all the molecules given in Table 2. The results are listed in Table 3 from the highest to lowest viscosity together with the values for DB_1, DB_2, and DB_3. For the shear viscosity trend prediction we can see that DB_1 is reliable only when there is a distinctive difference between the molecules in terms of number of branches. For example, it cannot predict a higher shear viscosity for Star100B6 and CombL52B4 which both have the same value for DB_1, and it cannot distinguish the differences between the H-shaped molecules. It is DB_2 that gives an accurate prediction of the shear viscosity trend that match the data. DB_3 also seems to predict the trend well except for one miss on star6. We would like to call DB_2 the "shape factor" that can be used as a universal parameter in defining the shear viscosity at least below the entanglement length for branched molecules in a non-Newtonian regime.

We found the shear thinning effect for all the molecules, although it was stronger for the linear-shaped molecules. For star-shaped molecules at high shear rates the shear thinning effect gets slightly weaker as the number of arms is increased. However, for comb-shaped molecules this is less obvious. For comb-shaped molecules we can see a plateau forming at lower shear rates, although it is hard to conclude that it is the Newtonian regime, and it seems the transition to shear thinning begins at lower shear rates. This can also be inferred from the order parameter results where we see that the tendency of the comb-shaped molecules to become ordered under shear is less than what is observed for the other molecules that we examined here. The results imply comb-shaped molecules are less susceptible to shear thinning. For the other molecules we cannot observe the onset of shear thinning, and it seems it begins at much lower shear rates. This is in contrast to our own simulations with shorter molecules of C_{30} in confined geometry. Also, experiments with low-density polyethylene (LDPE)[5] show increasing long-

chain branching induces shear thinning at lower shear rates, making the branched polymers more susceptible to shear thinning. Simulations on shorter C_{18} alkanes[10] also showed that star molecules show more resistance to shear thinning than their linear counterpart. However, in this work, for a highly branched molecule (similar to our comb molecules), the shear thinning behavior was similar to that observed for the linear molecule. In our simulations for star-shaped molecules the slope of the shear thinning line (given by α in Table 3) is one of the smaller ones. However, we cannot elaborate on the onset of shear thinning due to the lack of data in the Newtonian regime.

In a broader view, the first normal stress difference and normal stress difference ratio are also found to be mostly dependent on the effective length of the molecules. However, there are differences in the calculated N_1 for the molecules with the same effective length. Branching does not affect them much as long as they have the same effective length. An attempt to correlate N_1 to radius of gyration yields no conclusive results (refer to Table 3). However, we found that the shape of the molecule has an effect on the normal stress difference. This was demonstrated by the higher values for N_1 we obtained for H-shaped molecules. It seems an H-shaped molecule can conform its branches much easier in the flow field. At lower shear rates it exhibits lower normal stress differences and at higher shear rates N_1 will be more enhanced due to stretching of the arms at the end so that it effectively forms a longer molecule. However, for comb-shaped molecules changing the number of branches and their length does not change N_1 much. This is in contrast to the results of Wood-Adams,[5] experiments with LDPE where a higher first normal stress coefficient was correlated with increasing degree of branching. Sendijarevic and McHugh[14] conducted experiments with hyperbranched polymers of polyesters and poly(ether−imide). They observed the normal stress effect gets weaker with increasing degree of branching, obtaining lower exponent values for polymers with higher degrees of branching. We get the opposite picture in our simulations where (with the same type of molecule) generally β the exponent in the power law behavior of N_1 increases with increasing degree of branching. For the H-shaped molecules examined here we found that the results fit well in our analysis of the effect of degree of branching and effective molecular length. We found that the length of the branches does not affect the viscosity much, which is similar to experimental observations in work with the hyperbranched polyisobutylenes (PIB).[31] The H-shaped molecules we simulated here were simple, but we plan to simulate H-shaped molecules with multiple arms at the ends (a shorter replica of the so-called pom-pom model). We note again that the molecules simulated here are below the entanglement length, although we still capture some similarities observed in the behavior of these model molecules and real polymer melts.

References and Notes

(1) Crosby, B. J.; Mangnus, M.; de Groot, M.; Danniel, R.; McLeish, T. C. B. *J. Rheol.* **2002**, *46*, 401.
(2) Wood-Adams, P. M.; Dealy, J. M. *J. Rheol.* **1996**, *40*, 761.
(3) Garbassi, F.; Gila, L.; Proto, A. *Polym. News* **1994**, *19*, 367.
(4) Vega, F.; Muñoz-Escalona, A.; Santamaría, A.; Muñoz, M. E.; Lafuente, P. *Macromolecules* **1996**, *29*, 960.
(5) Wood-Adams, P. *J. Rheol.* **2001**, *45*, 203.
(6) McLeish, T. C. B.; Larson, R. G. *J. Rheol.* **1998**, *42*, 81.
(7) McLeish, T. C. B. *Macromolecules* **1988**, *21*, 1062.
(8) McLeish, T. C. B.; O'Connor, K. P. *Polymer* **1993**, *34*, 2998.
(9) Daivis, P.; Evans, D. *J. Chem. Phys.* **1992**, *97*, 616.
(10) Kioupis, L. I.; Maginn, E. J. *J. Phys. Chem. B* **1999**, *103*, 10781.
(11) Kioupis, L. I.; Maginn, E. J. *J. Phys. Chem. B* **2000**, *104*, 7774.
(12) Khare, R.; de Pablo, J.; Yethiraj, A. *J. Chem. Phys.* **1997**, *107*, 6956.
(13) Jabbarzadeh, A.; Atkinson, J. D.; Tanner, R. I. *Tribol. Int.* **2002**, *35*, 35.
(14) Sendijarevic, I.; McHugh, A. J. *Macromolecules* **2000**, *33*, 590.
(15) Evans, D. J.; Morris, G. P. *Comput. Phys. Rep.* **1984**, *1*, 297.
(16) Evans, D. J.; Morris, G. P. *Statistical Mechanics of Non-Equilibrium Liquids*; Academic Press: New York, 1990.
(17) Lees, A. W.; Edwards, S. F. *J. Phys. Ser. C* **1972**, *5*, 1921.
(18) Travis, K. P.; Daivis, P. J.; Evans, D. J. *J. Chem. Phys.* **1995**, *103*, 10638.
(19) Ryckaert, J. P.; Bellemans, A. *Chem. Phys. Lett.* **1975**, *30*, 123.
(20) Smit, B.; Karaborni, S.; Siepmann, I. *J. Chem. Phys.* **1994**, *102*, 2126.
(21) Siepmann, J. I.; Martin, M. C.; Mundy, C. J.; Klien, M. L. *Mol. Phys.* **1997**, *90*, 687.
(22) Cui, S. T.; Cummings, P. T.; Cochran, H. D. *Fluid Phase Equilib.* **1997**, *141*, 45.
(23) Moore, J. D.; Cui, S. T.; Cochran, H. D.; Cummings, P. T. *J. Non-Newtonian Fluid Mech.* **2000**, *93*, 83.
(24) Mondello, M.; Grest, S.; Webb, E. B., III.; Paczak, P. *J. Chem. Phys.* **1998**, *109*, 798.
(25) Jabbarzadeh, A.; Atkinson, J. D.; Tanner, R. I. *Comput. Phys. Commun.* **1997**, *107*, 123.
(26) Jabbarzadeh, A.; Atkinson, J. D.; Tanner, R. I. *Comput. Phys. Commun.* **2003**, *150*, 65.
(27) Irving, J. H.; Kirkwood, J. G. *J. Chem. Phys.* **1950**, *18*, 817.
(28) Fetters, L. J.; Kiss, A. D.; Pearson, S. D.; Quack, G. F.; Vitus, F. J. *Macromolecules* **1993**, *26*, 647.
(29) Tanner, R. I. *Engineering Rheology*, 2nd ed.; Oxford University Press: New York, 2000.
(30) Wood-Adams, P. M.; Dealy, J. M.; deGroot, A. W.; Redwine, O. D. *Macromolecules* **2000**, *33*, 7489.
(31) Robertson, C. G.; Roland, C. M.; Puskas, J. E. *J. Rheol.* **2002**, *46*, 307.
(32) Rouse, P. E. *J. Chem.Phys.* **1953**, *21*, 1272.

MA025782Q